Design 3D printing cementitious materials via Fuller Thompson theory and Marson-Percy model

Yiwei Weng[a,b], Mingyang Li[a], Ming Jen Tan[a], Shunzhi Qian[a,b]

a, Singapore Centre for 3D Printing, School of Mechanical and Aerospace Engineering, Nanyang Technological University, Singapore

b, School of Civil and Environment Engineering, Nanyang Technological University, Singapore

Abstract:

Cementitious materials for 3D printing have special requirements for rheological properties, which are significantly affected by many factors, including sand gradation and packing fraction. Fuller Thompson theory and Marson-Percy model are classic approaches for sand gradation and packing fraction optimization, respectively. This paper attempts to apply Fuller Thompson theory and Marson-Percy model in designing cementitious materials for 3D Cementitious Materials Printing (3DCMP). Various gradation methods adopted in this study were Fuller Thompson gradation (mixture A), uniform-gradations (mixture B and C), gap-gradations (mixture D and E). Besides these mixtures with special gradation approaches, one mixture using natural river sand (mixture F) was prepared as well. Rheological properties were characterized by static/dynamic yield stress and plastic viscosity in Bingham Plastic model. Buildability was examined by printing a column with 10 cm inner diameter via a gantry printer. Rheological test results indicate that mixture A designed by continuous gradation possesses the highest static/dynamic yield stress and lowest plastic viscosity. During printing test for buildability, mixture A can easily reach up to 40 layers without notable deformation, while all other mixtures deformed noticeably and fell down before the 35th layer. Finally, a large-scale printing was

carried out with mixture A and a structure with the height of 80 cm was printed successfully without notable deformation. Density, compressive strength and flexural strength of printed filaments were also characterized. Mechanical performance test results illustrate mixture A has the highest density and appropriate compressive strength, and a relative high flexural strength at different curing ages. These results indicate that Fuller Thompson theory and Marson-Percy model can serve as a reasonable guide for material rheology design for 3DCMP.

Key words: Fuller Thompson theory; Marson-Percy model; 3D cementitious materials printing; Bingham Plastic model

1 Introduction

3D Printing, also referred to as Additive Manufacturing, is a technology which builds a solid part via a layer-by-layer process [1]. Due to its advantages such as customized production, reduced waste, and diminished lead-time of rapid prototype [2], 3D Printing has attracted much attention from various fields including building and construction [3]. In the last decade, much research has been conducted in the field of 3D Printing for Building and Construction, especially in the development of printing systems such as Mortar Printing [3–5], FreeFab [6], Contour Crafting [7–9] and Robotic printing system [10,11]. While most of the 3D Printing for Building and Construction processes can be classified as 3D Cementitious Materials Printing (3DCMP), little research has been done on how to design materials for 3DCMP [12–14], especially from the aspect of material design methods for 3DCMP.

Materials used in 3DCMP need to meet certain specific rheological requirements [3,15]. The most essential steps in 3DCMP are conveying mixed materials to the nozzle via a delivery system and depositing materials to build the solid object in a layer-by-layer manner. In the conveying step, the materials are required to have good pumpability, which indicates how easily

material can be conveyed; and in the deposition step, the materials are required to have good buildability, which indicates how well the materials can be stacked stably. Both pumpability and buildability are closely related to the rheology performance of materials, namely static/dynamic yield stress and plastic viscosity. Static yield stress is the minimum shear stress required to initiate the flow and dynamic yield stress is the critical shear stress below which the shear stress is insufficient to maintain the flow. Plastic viscosity is the resistance of a fluid to flow when the fluid is flowing. All these rheological properties are attributed to the inter-particle force [16]. Typically, higher static/dynamic yield stress and plastic viscosity would enhance buildability and hinder pumpability [17] and thus, seeking a balance between buildability and pumpability is critical in material rheology design for 3DCMP.

It is well known that aggregates take up 60-80% of the total volume of cementitious materials, the most commonly used building and construction material worldwide[19]. Rheological properties of cementitious material are highly affected by the gradation of aggregate [18–20]. Good aggregate gradation contributes to high density and proper rheological properties of materials. Fuller Thompson theory is a classic theory for gradation design. In 1907, W.B Fuller and S.E. Thompson proposed a theory for gradation design based on experimental results[21]. Later, Federal Highway Administration (FHWA) proposed a modified Fuller Thompson equation [22]. Fuller Thompson theory has been widely used in producing high performance concrete [20,23], designing sustainable concrete with minimum content of cement [24] and optimizing rheology [25].

Rheological performance is significantly affected by the packing fraction of a system as well, which is defined as the ratio of solids to the total volume. Theoretically, materials designed by the continuous gradation can achieve maximum packing fraction, which describes a condition

where the void volume reaches minimum for a given system. According to Marson-Percy model [26], the highest packing fraction of materials results in the lowest plastic viscosity.

To fulfill the material rheological property requirements in 3DCMP, Fuller Thompson theory and Marson-Percy model were applied in materials design of 3DCMP. Six different mixtures were prepared with different gradation approaches using five different sands (0.6-1.2 mm, 0.25-0.6 mm, 0.15-0.25 mm, less than 0.15 mm and natural river sand), i.e. mixture A designed by Fuller Thompson theory, mixture B and C designed by uniform-gradations, mixture D and E designed by gap-gradations and mixture F using natural river sand without special gradation design. Rheological tests were carried out to investigate the fresh performance of all mixtures, and printing tests for buildability were conducted among different mixtures via a gantry printer. Density and mechanical performance (compressive and flexural properties) were characterized as well. It should be noted that the time and temperature effect of rheological/material properties is not considered due to the limited scope of this study. Furthermore, all tests including printing are conducted within 30 minutes of cement mixing and under constant lab temperature of 26**°C**.

2 Theory

2.1 Built-up theory and Bingham model

Perrot et al. established the relation between static yield stress and buildability of 3DCMP [17]. The simplified relation is expressed as follows:

$$H = \frac{\alpha}{\rho g}\tau_s \quad (1)$$

where H (m) and α are the printed height (buildability) and the geometric factor [17] of printed structure respectively; ρ (g/cm^3) and g (m/s^2) are the density of materials and gravitational

constant respectively. τ_s (Pa) is the static yield stress, which is corresponding to static torque in Fig. 1

Fig. 1 presents the typical rheological test result via a Schleibinger Viskomat XL rheometer with vane probe. The static yield stress can be converted from the maximum torque (also referred to as static torque) in the ascending curve. Based on linear fitting of descending curve, its slop and intersection with Y axis are defined as torque viscosity and flow resistance respectively, which can then be converted into plastic viscosity and dynamic yield stress in Bingham Plastic model.

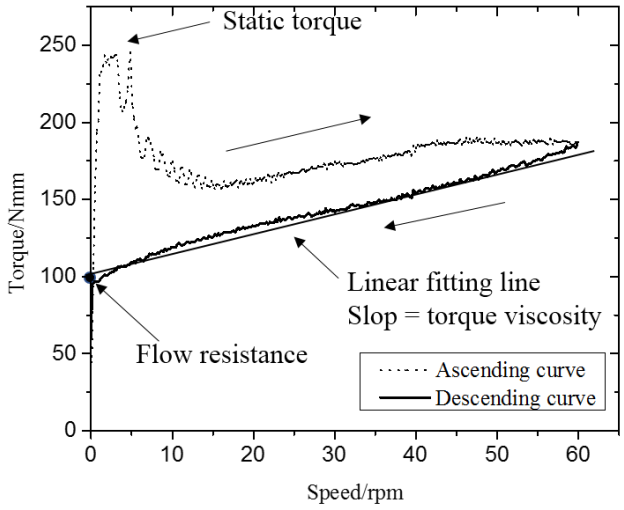

Fig. 1 Typical rheological test result

Bingham Plastic model is widely accepted to describe the rheological property of cementitious materials [27–33], which has the shear stress τ (Pa) expressed as

$$\tau = \tau_d + k\dot{\gamma} \tag{2}$$

where τ_d (Pa) and k (Pa s) are dynamic yield stress and plastic viscosity, respectively. $\dot{\gamma}$ (1/s) is the shear rate.

From Eq.(1), the buildability is proportional to the static yield stress. It should be noted that in this study, the rheological properties are assumed to be constant during the whole printing process as the time consumed for printing test (around 2 minutes) is much shorter than rheological test (10 minutes). The effect of time on the rheological performance, printability and buildability will be investigated in the future. It also worth noting that in this study, we focus on the effect of yield stress and plastic viscosity on the printability and buildability and the thixotropic behaviour and the rate of re-flocculation are out of our scope.

Generally, materials' pumpability is reflected by pumping pressure during pumping process, which is related to Bingham Plastic parameters as well. The relationship can be described by [34]

$$P = \left(\frac{8\tau_d}{3R} + \frac{8k}{\pi R^4} Q \right) L \tag{3}$$

where P (Pa) is the pumping pressure. L (m) and R (m) are the length and radius of pipe, respectively. Q (m^3/s) is the average flow rate. In this case, R is much less than 1 m, which means that plastic viscosity (k) possesses more significant effect on the pumping pressure, compared with dynamic yield stress (τ_d). Eq. (3) shows that the increases of dynamic yield stress and plastic viscosity augment the pumping pressure of cementitious material for specific pipe and flow conditions, which reduces the pumpability of cementitious material. Therefore, a low plastic viscosity is required for cementitious materials to decrease the pumping pressure, which will facilitate a safe and economic operation of pumping/printing process.

2.2 Fuller Thompson theory and Marson-Percy model

Gradation is an important attribute to produce economical cementitious materials with maximum density and minimum void content. Sand gradation formula proposed via W.B. Fuller and S.E Thompson is expressed as following [21]

$$p_i = \left(\frac{d_i}{D} \right)^{0.5} \quad (4)$$

where p_i is the percent pass i^{th} sieve, d_i (mm) is the opening size of i^{th} sieve, and D (mm) is the maximum particle size. Later, in 1962, FHWA published a modified version for Fuller's equation

$$p_i = \left(\frac{d_i}{D} \right)^{0.45} \quad (5)$$

Three types of gradation are schematically shown in Fig. 2. Applying Fuller Thompson equation in sand gradation design forms a continuous gradation, in which interaction between particles exists at many points of contact and realizes a maximum densified system. Gap gradation is designed via missing a certain range of sand particle size in the paste, which possesses more voids content and less contact points compared with the continuous grading system. Using single size sand in the mixture can achieve uniform gradation mixture which has minimum contact points between particles. Since contact points contribute to the friction in the mixture, increasing the contact points between particles can raise the friction and, thus, resulting in increased static yield stress to initiate flow and dynamic yield stress to maintain the flow.

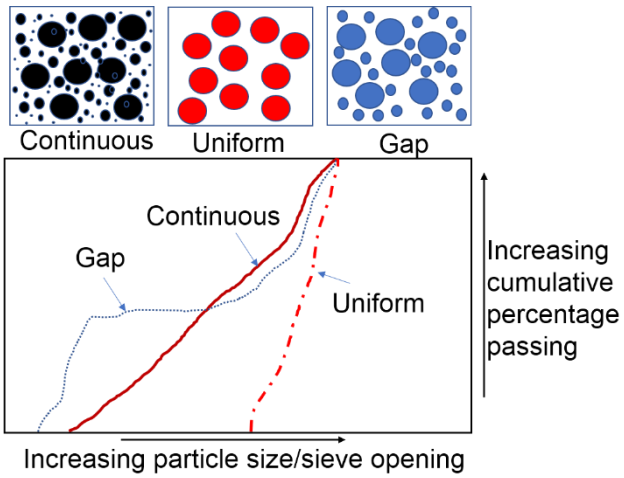

Fig. 2 Three types of sand gradation

Shear viscosity μ is affected by packing fraction ϕ, maximum packing fraction ϕ_m and shear rate $\dot{\gamma}$. The relationship between packing fraction, shear rate and shear viscosity is commonly expressed by Marson-Percy model [26]

$$\mu(\phi,\dot{\gamma}) = \left(1-\frac{\phi}{\phi_m}\right)^{-2} \mu_b(\dot{\gamma}) \tag{6}$$

where $u_b(\dot{\gamma})$ (Pa s) is the shear viscosity of the binder, which is the same among all samples. In our study, ϕ is kept as a constant and ϕ_m is variable for mixtures with different gradation. Theoretically mixture designed by Fuller Thompson theory can achieve a maximum density and minimum void system, which means ϕ_m is the maximum among all mixtures, it should possess the lowest shear viscosity μ.

The relation between shear viscosity and plastic viscosity of Eq. **Error! Reference source not found.** can also be expressed as follows:

$$\mu = k + \frac{\tau_d}{\dot{\gamma}} \tag{7}$$

Fuller Thompson theory indicates that when the mixture designed by Eq. (4), it possesses the highest dynamic yield stress (τ_d) and lowest shear viscosity (μ from Eq. (6)) among all mixtures. Therefore, Eq. (7) indicates that the plastic viscosity (k) of mixture designed by Eq. (4) is the smallest as well when the shear rate is the same among different mixtures. As mentioned before, a low plastic viscosity is required for cementitious materials to decrease the pumping pressure, which will facilitate a safe and economic operation of pumping/printing process.

3 Materials, and mixture proportion

3.1 Materials

Mixtures in this study consist of Ordinary Portland Cement (OPC, ASTM type I, Grade 42.5), silica fume (SF, undensified, Grade 940, Elkem company), silica sand, fly ash (FA, Class F), natural river sand, water and superplasticizer (SP). Fig. 3 illustrates the particle size distribution of cement, SF and FA, which were analyzed by Mastersizer 2000. Table 1 illustrates the chemical composition of OPC and FA, respectively. Silica sand with four different sizes, i.e., 0.6-1.2 mm, 0.25-0.6 mm, 0.15-0.25 mm, and less than 0.15 mm, were used in this study, either as mono-sized ingredient or a mixture of all four.

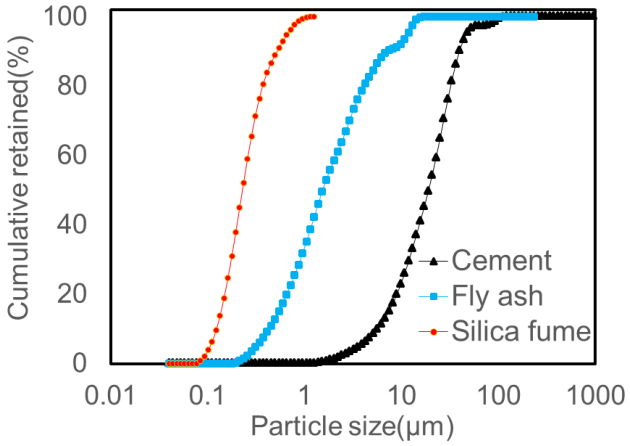

Fig. 3 Particle size distribution of OPC, FA and SF

Table 1 Chemical composition of fly ash and Ordinary Portland Cement (OPC)

Formula	Concentration / %	
	Fly ash	Cement
SiO_2	58.59	24.27
Al_2O_3	30.44	4.56
Fe_2O_3	4.66	3.95
TiO_2	2.02	0.55
K_2O	1.51	0.61
CaO	1.21	62.2
MgO	0.776	3.34
P_2O_5	0.531	0.15
Na_2O	-	0.21
SO_3	0.0914	-
ZrO_2	0.04	-
MnO	0.0351	-
Cr_2O_3	0.027	-
CuO	0.0254	-
ZnO	0.0229	-

3.2 Mixture proportion

Six different mixtures, including five mixtures with silica sands following different gradation and one mixture with natural rive sand, were used in this study. The sand gradation curves are shown in Fig. 4. Sand for mixture A followed the Fuller Thompson theory to achieve a continuous gradation system. The continuous gradation mixture used in this study is 39. 23% of sand size less than 0.15 mm, 10.14% of sand with 0.15-0.25 mm, 23.84% of sand with 0.25-0.6

mm, and 26.80% of sand with 0.6-1.2 mm. Sand for mixture B was a uniform gradation mixture with sand size ranging from 0.6 mm to 1.2 mm. Sand for mixture C was another uniform gradation mixture with sand size ranging 0.15 -0.25 mm.

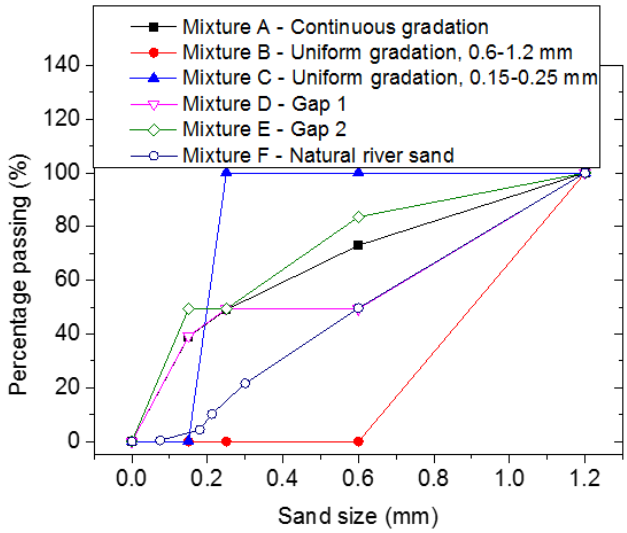

Fig. 4 Sand gradation curves for different mixtures

As can been seen from Fig. 4, the gap gradation 1 (mixture D) used in this study removed the sand particle size between 0.25-0.6 mm, and was composed of 39. 23% of sand particle size less than 0.15 mm, 10.14% of sand particle size with 0.15-0.25 mm, and 50.63% of sand particle size with 0.6-1.2 mm. Gap gradation 2 (mixture E) removed sand particle size between 0.15-0.25 mm, and is composed of 49.37% of sand particle size less than 0.15 mm, 23.84% of sand particle size with 0.25-0.6 mm, and 26.69% of sand particle size with 0.6-1.2 mm.

Mixtures F used the natural river sand as the raw materials while the sand with particle size bigger than 1.2 mm was sieved out. Sieved natural river sand was then analyzed by sieving machine. The sieved natural rived sand consists of 0.86% of sand with particle size less than 0.075 mm, 6.99% of sand ranging from 0.075 to 0.18 mm, 3.68% of sand ranging from 0.18 to

0.212 mm, 11.24% of sand ranging from 0.212 to 0.3 mm, 32.87% of sand ranging from 0.3 to0.6 mm and 44.36% of sand ranging from 0.6 to1.2 mm, as shown in Fig. 4.

All the mixtures mentioned above, except silica sand itself and natural river sand, followed the same mixture proportion, as shown in Table 2:

Table 2 Mixture proportion

OPC	Sand	W	FA	SF	SP/(g\L)
1	0.5	0.3	1	0.1	1.3

Note: all ingredients content are expressed as weight proportion of cement content

4 Mixing and Testing Procedures

4.1 Mixing procedures

A hobart mixer X200L was used for mixing. Since many factors can affect the rheological properties of cement slurries, such as mixing time, mixing speed and temperature [35], the mixing procedures in this study were fixed to minimize the differences among batches. Firstly, the powder of all solid ingredients was dry mixed for 3 minutes in stir speed; then water was added, the mixing process continued for 3 minutes in stir speed followed by 2 minutes in speed I; and then the SP was added, the mixing process continued for 1 minute in stir speed followed by 3 minutes in speed I.

4.2 Rheological characterization

Rheological properties of mixed materials were evaluated via Viskomat XL and mini-slump. The six-blade vane probe and cage used for rheological test to avoid slippage of cement paste. Both the diameter and the height of this vane probe are 69 mm, and the gap between probe and cage, and the bottoms of probe and barrel are both 40 mms. During the rheological test, the speed of rheometer is increased linearly from 0 rpm to 60 rpm in 5 minutes. Afterwards, it is decreased

linearly to 0 rpm in another 5 minutes as shown in Fig. 5. Then the static/dynamic yield stress and plastic viscosity can be computed by Chhabra et al [34]:

$$\Gamma = \frac{4\pi R_1^2 R_2^{\ 2} l\eta}{R_2^{\ 2} - R_1^{\ 2}}\omega_2 - \frac{4\pi R_1^2 R_2^{\ 2} l\tau_0}{R_2^{\ 2} - R_1^{\ 2}}\ln\frac{R_1}{R_2} \tag{8}$$

where Γ (N m) is the torque, ω_2 (rad/s) is the rotational speed of outer barrel, l (m) and R_1 (m) are the length and radius of the probe, respectively, and R_2 (m) is the radius of outer barrel. For the static yields stress, it can be directly obtained by applying static torque in Eq. (8).

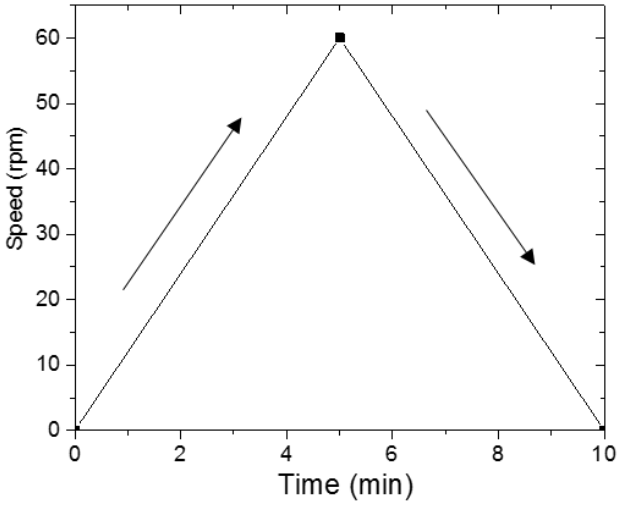

Fig. 5 Rheological testing programs

Mini-slump test is a classic method to measure materials' workability , which is based on the spread diameter of slurry placed into a cone-shape mold [37]. The mini slump cone typically has a height of 70 mm, an internal diameter of 50 mm and 100 mm at the top and bottom, respectively. The cone is placed on a flat, level, and non-absorbent hard surface. During the test, it is filled with fresh material, and then raised after certain amount of time to allow the material to spread. After spreading ceases, two diameters of material mass are measured in orthorginal

direction, and the workability of cementitiou material can be characterized by the average of the two diameters.

4.3 Printing investigation

Finally, printing tests were conducted to investigate the buildability of different mixtures. As shown in Fig. 6, a gantry printer with a 1.2 m × 1.2 m × 1.0 m (L×W×H) printing volume was used to control nozzle position for printing. As shown in Fig. 7, the materials were pumped by a MAI Pictor pump from black funnel to the nozzle head through a hose with 3 m in length and 2.54 cm in diameter. Fig. 8 illustrates the 3D model used in the printing test. The circular column with 10 cm inner diameter is composed of 50 layers. Each layer is 20 mm in width and 10 mm in height theoretically.

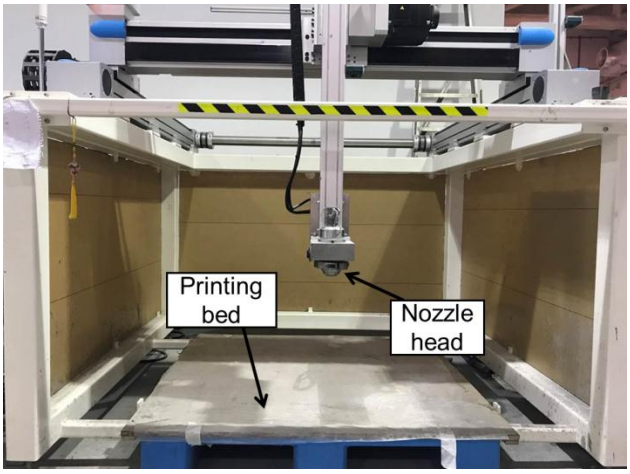

Fig. 6 Gantry concrete -printer used for printing test

Fig. 7 MAI Pictor pump to convey materials

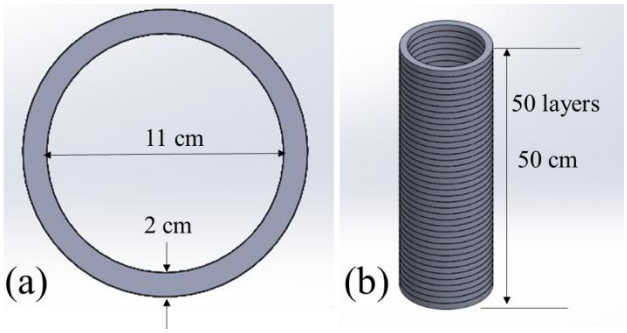

Fig. 8 3D model for printing test

4.4 Density, compressive strength and flexural performance

All six mixtures were casted into 50 mm × 50 mm × 50 mm cubic molds, consolidated via vibration table and trowel finished. All specimens were then demolded after 24 h. All samples were covered by a plastic sheet and then stored into a plastic container for curing. The density was tested at 7 days, 14 days and 28 days, according to ASTM C642 [38].

After density test, the compressive strength test was carried on the cubic specimens. The compressive strength was measured by uniaxial loading in triplicates at 7, 14 and 28 days in

accordance with the specifications of ASTM C109/C109M-13 [39]. The equipment used for this purpose was a Toni Technik Baustoffprüfsysteme machine with a loading rate of 100 KN/min.

The gantry concrete printer was used to fabricate flexural specimens. The nozzle used for printing was 30 mm × 15 mm (L × W). The printing speed and pumping speed were 4,000 mm/min and 1.8 L/min respectively. The standoff distance was 15 mm for each layer. Printed path and side view of printed filaments are shown in Fig. 9. Then, printed specimen was cut into separate filaments with 350 mm in length and 300 mm in height (two layers). Afterwards, a four-point bending test with a span length of 240 mm was conducted at 7 days, 14 days and 28 days.

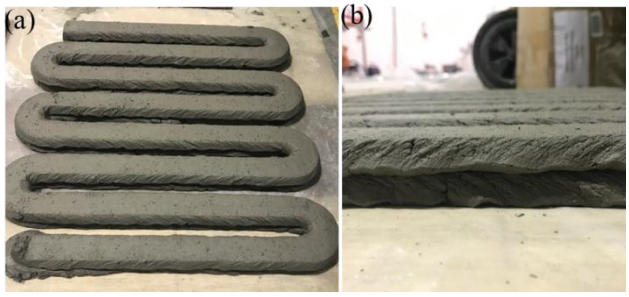

Fig. 9 Flexural specimen preparation: (a) top view of the printed filament; (b) side view of printed filament

5 Results and Discussion

5.1 Rheological analysis

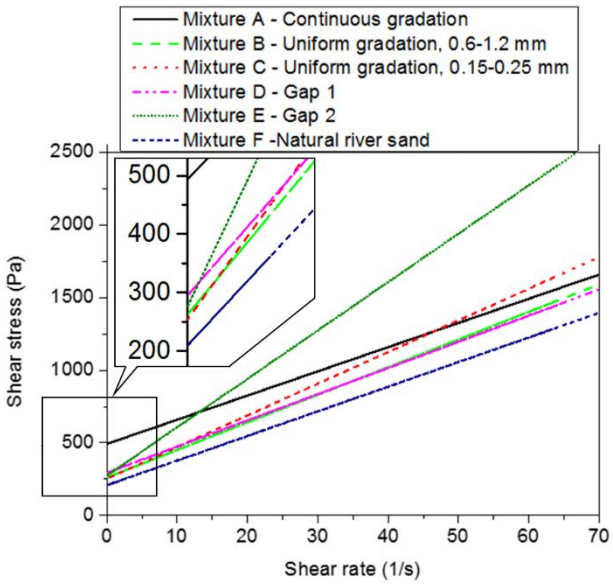

Fig. 10 illustrates the shear stress and shear rate relation from rheological results based on Bingham Plastic model. The raw data of static torque, flow resistance and torque viscosity were shown in Table 3, which were then converted to static/dynamic yield stress and plastic viscosity via Eq.(8) and shown in the same table.

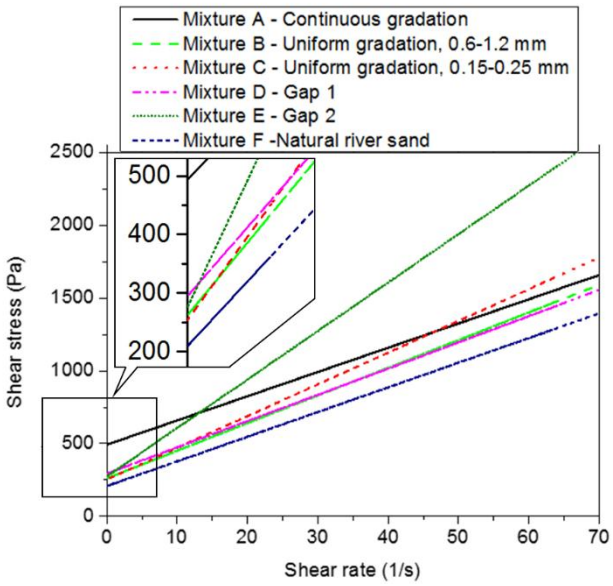

295
296 *Fig. 10 Shear stress and shear rate relation based on Bingham model*
297

298 *Table 3 rheological performance of different mixtures*

	Static torque/ N·mm	Flow resistance/ N·mm	Torque viscosity/ (N·mm/rpm)	Static yield stress/Pa	Dynamic yield stress/ Pa	Plastic viscosity/ Pa·s
Mixture A	3390	498.5	2.280	3350	492.7	16.65
Mixture B	2440	264.5	2.601	2411	261.3	19.00
Mixture C	2132	255.8	2.984	2107	252.8	21.81
Mixture D	3358	287.3	2.941	3318	290.6	18.03
Mixture E	2725	277.4	4.560	2693	274.1	33.31
Mixture F	1897	210.9	2.320	1874	208.4	16.95

299

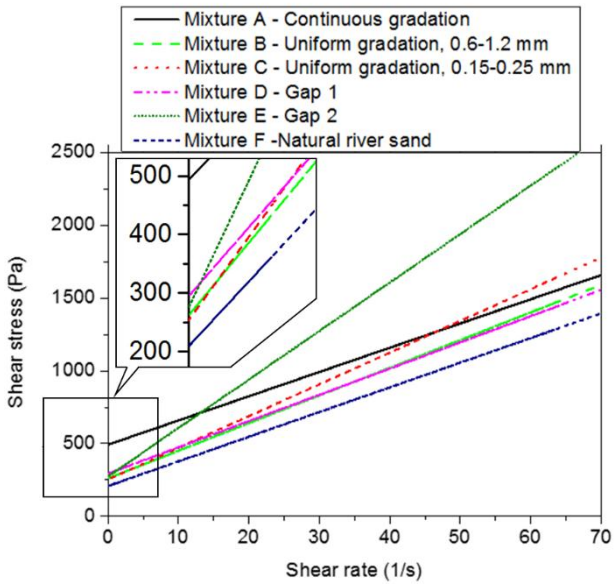

As can be seen from Fig. 10 and Table 3, mixture A has the highest static yield stress and the smallest plastic viscosity, which is very desirable to ensure low pumping pressure and high buildability based on previous discussion; mixture E possesses a highest viscosity among all the mixtures, which suggests that the pumpability of mixture E could be the worst.

Fig. 11 reveals the results from mini-slump test. As can be seen from Fig. 11, for all mixtures, the diameter tends to decline along the time. At each time point, mixture A has the lowest slump. After 20 minutes, the spread diameter of mixture A is approximately 100 mm.

Rheological and mini-slump test results indicate that the most proper materials for 3DCMP is mixture A with continuous gradation. With the highest yield stresses and the lowest plastic viscosity, mixture A is expected to reveal better pumpability and buildability among all mixtures investigated in this study.

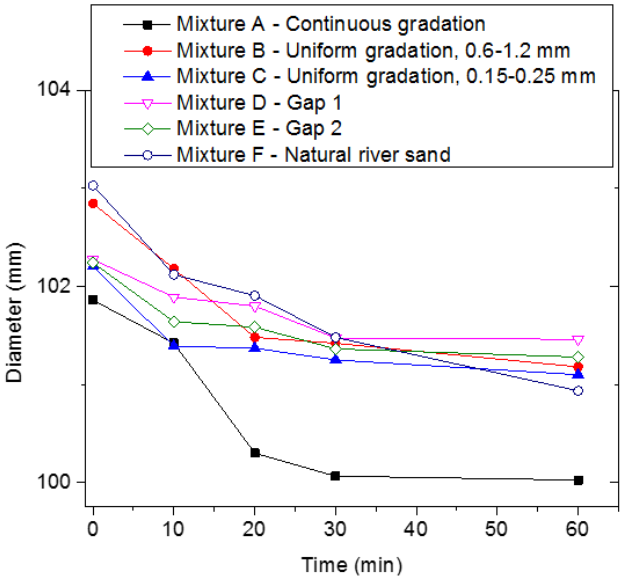

Fig. 11 Mini-slump test result

5.2 Printing Test

A gantry printer system was used to conduct the printing test of mixtures A to F. Moving speed of nozzle and pumping speed of were 9,000 mm/min and 1.8 L/min, respectively. During the printing test, the printed part can maintain its shape initially. When the printed structure meets the failure criteria at the fresh state, which was described by Perrot et al. [26], suddenly noticeable deformation occurs. This was followed by misalignment of printing path and final collapse of the printed structure. The layer numbers with noticeable deformation and final collapse were recorded during the printing test.

Printing test results are summarized in Table 4, where layer number associated with noticeable deformation and final collapse are presented. Taking mixture A as an example, it maintained its shape until the 42nd layer (Fig. 12 (a)), followed by large deformation (Figure 12(b)) and finally fell down at the 43rd layer (Fig. 12 (c)). For other mixtures, similar phenomena are observed during the printing test, except that they all showed large deformation and collapsed at much

early stage (smaller layer number). As stated by Perrot et al. [17], the maximum build-up height can be computed by solving equation Eq. (1). For hollow cylinder, the geometric factor can be computed by

$$
\begin{aligned}
\alpha = {} & \left(R_2^2 - R_1^2\right)^{-1}\left(\frac{1}{2}+\frac{C_\alpha}{R_2^2}\right)^{-1}\sqrt{\frac{3}{4}+\frac{C_\alpha^2}{R_2^4}} \\
& \cdot\left\{\frac{4}{H}\left[\frac{\left(R_2^3 - R_1^3\right)}{6}+C_\alpha\left(R_2 - R_1\right)\right]\right. \\
& +2C_\alpha\left(\sqrt{\frac{3R_2^4}{4C_\alpha^2}+1}-\sqrt{\frac{3R_1^4}{4C_\alpha^2}+1}\right) \\
& -2C_\alpha\left[\operatorname{arcsinh}\left(\frac{2C_\alpha}{\sqrt{3}R_2^2}\right)-\operatorname{arcsinh}\left(\frac{2C_\alpha}{\sqrt{3}R_1^2}\right)\right] \\
& -2R_1^2\left(\frac{3}{4}+\frac{C_\alpha^2}{R_1^4}\right)^{-1/2}\left(\frac{1}{4}-\frac{C_\alpha^2}{R_1^4}\right) \\
& \left.-2R_2^2\left(\frac{3}{4}+\frac{C_\alpha^2}{R_2^4}\right)^{-1/2}\left(\frac{1}{4}-\frac{C_\alpha^2}{R_2^4}\right)\right\}
\end{aligned}
\tag{9}
$$

where C_α can be solved from equation

$$
\frac{\frac{1}{2}-\frac{C_\alpha}{R_2^2}}{\sqrt{\frac{3}{4}+\frac{C_\alpha^2}{R_2^4}}}-\frac{\frac{1}{2}-\frac{C_\alpha}{R_1^2}}{\sqrt{\frac{3}{4}+\frac{C_\alpha^2}{R_1^4}}}+\operatorname{arcsinh}\left(\frac{2C_\alpha}{\sqrt{3}R_2^2}\right)-\operatorname{arcsinh}\left(\frac{2C_\alpha}{\sqrt{3}R_1^2}\right)=0 \tag{10}
$$

The detailed derivation process following geometric factor for cylinder derived by Roussel and Lanos [40] is enclosed in Appendix A. The comparison between prediction and experimental maximum built-up heights is shown in Fig. 13. As can be seen from Fig. 13, the model can well predict the deformation/collapse layer number. It is worth noting that the derivation of predicted and actual result of mixture D is quite big. As the plastic viscosity of D is high, it reduces the

printability and causes the discontinuity during the printing test, which reduces the stability of printed structure.

Table 4 Summary of the layer number during which noticeable deformation and final collapse occurred

	layer number with noticeable deformation	layer number with final collapse
Mixture A	42nd	43rd
Mixture B	30th	31st
Mixture C	27th	32nd
Mixture D	31st	36th
Mixture E	32nd	34th
Mixture F	24th	25th

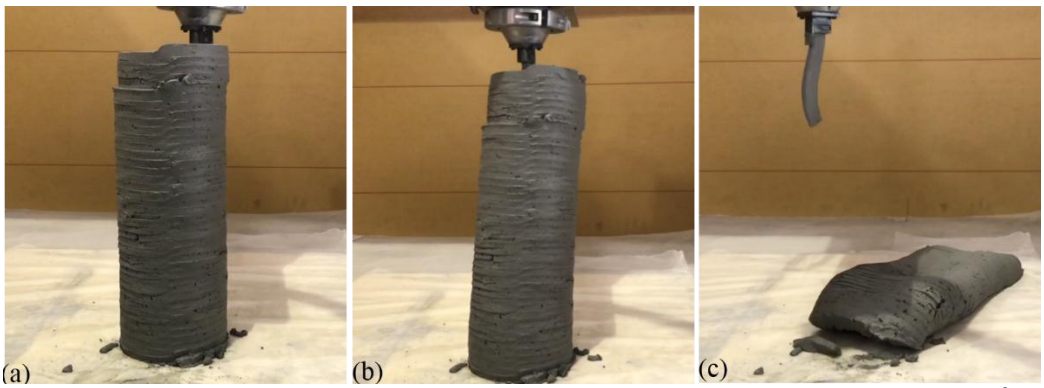

Fig. 12 The printing test result of mixture A: (a) maintained the shape untile 42nd layer; (b) sudden deformation at the 42nd layer and (c) fell down at 43rd layer

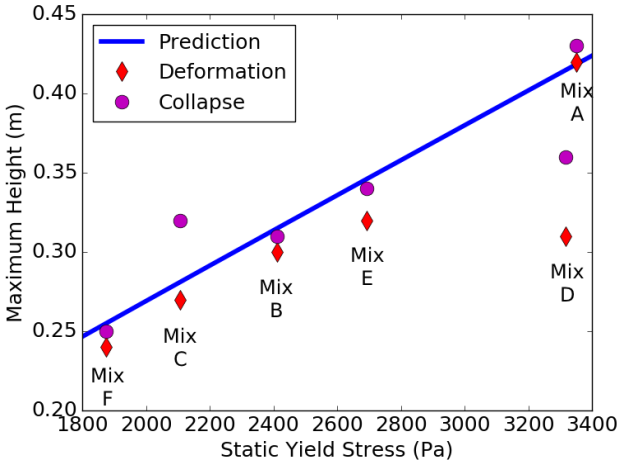

352

353 *Fig. 13. Comparison between prediction and experimental maximum built-up heights*

354

355 Afterwards, a large printing test was conducted using mixture A. A circular nozzle with 20 mm
356 in diameter was used in this printing. Moving speed of nozzle and pumping speed of pump were
357 9,000 mm/min and 1.8 L/min, respectively. 3D printing model is shown in Fig. 14. As can be
358 seen from the top-view of the 3D model (Fig. 14 a), it is composed of 4 semicircles and 4 quarter
359 circles with 10 cm in diameter and 2 cm in thickness. Then the total layer numbers are 80 for
360 printing and the layer height is 10 mm (Fig. 14 b). The final printed part is shown in Fig. *15*.

361

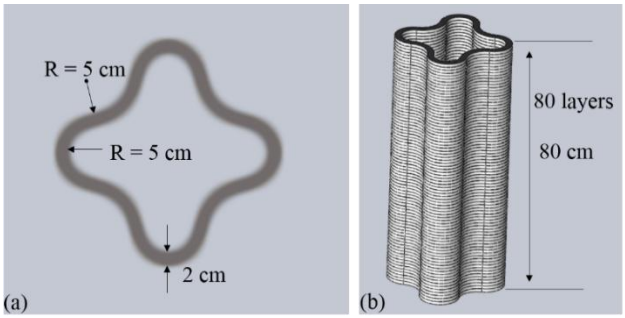

362
363 *Fig. 14 3D model for large-scale printing: (a) top-view; (b) side-view*
364

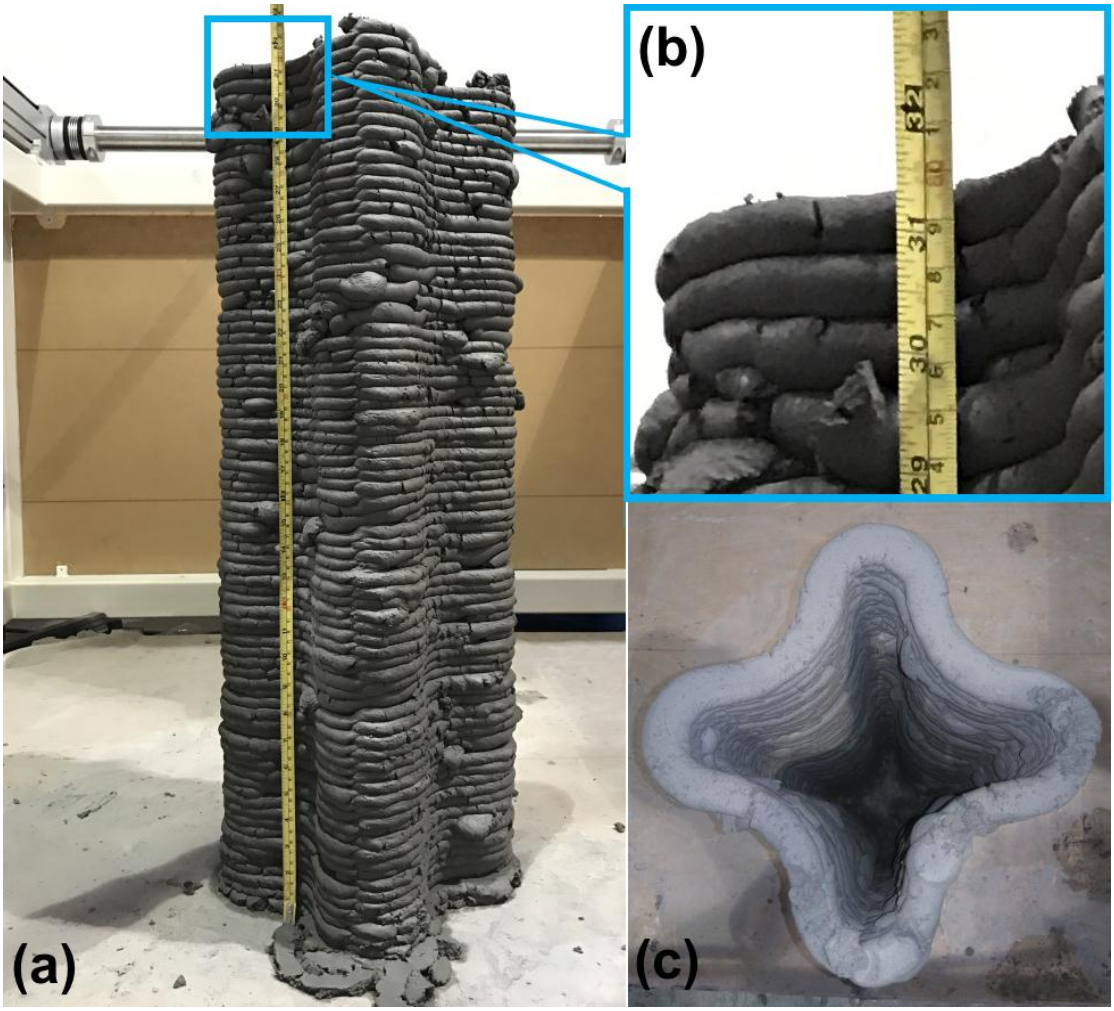

Fig. 15 Gantry printed part: (a)final printed part; (b) height and layer thickness and (c) top view of the printed part

5.3 Density, compressive strength and flexural strength

The density of cementitious material is related to its packing. Better packing from continuous gradation yields high density. The result of density of all mixtures is shown in Fig. 16. As expected, mixture A possesses the highest density among all mixtures at 7 days, 14 days and 28 days. Furthermore, the density of all mixtures also increases with time.

Fig. 17 and 18 present the result of the compressive strength and flexural strength of all mixtures. Mechanical strength of all mixtures increases with time as expected. Mixture A possesses

appropriate compressive and flexural strength at 28 days, which are 49.7 MPa and 3.73 MPa respectively.

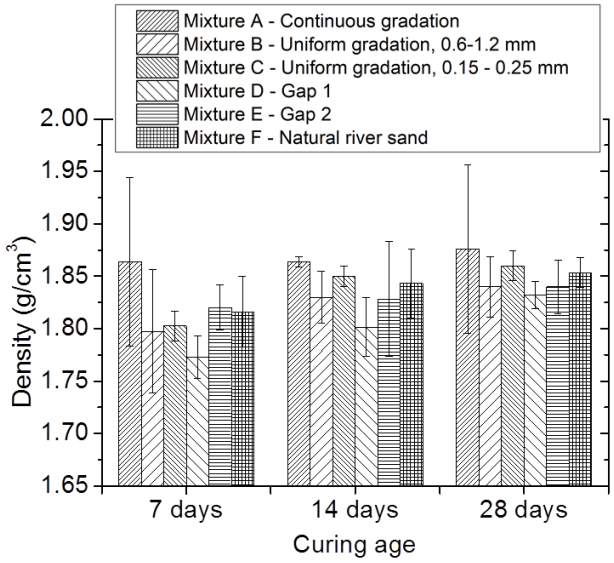

Fig. 16 Density of all mixtures

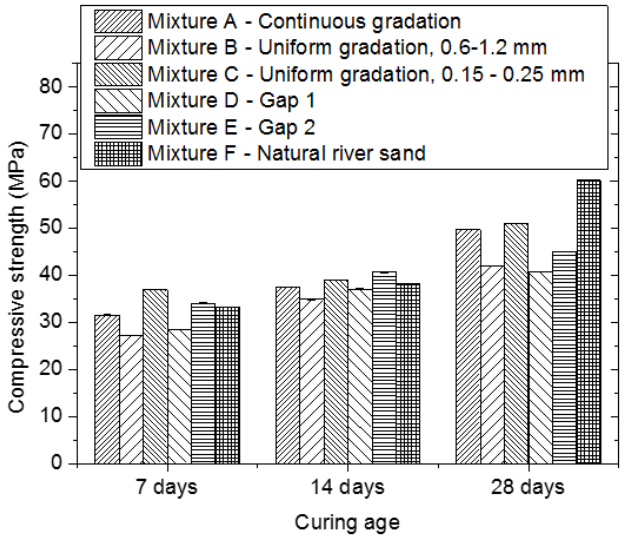

Fig. 17 Compressive strength of all mixtures

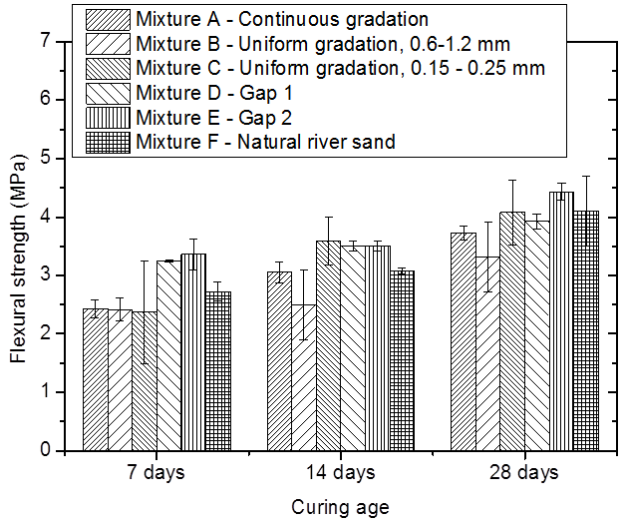

Fig. 18 Flexural strength of different mixtures

6 Summary and Conclusion

3DCMP requires the material to have low plastic viscosity and high yield stresses to meet the requirements for both pumpability and buildability. Fuller Thompson theory and Marson-Percy model were adopted as a guideline to design construction materials with proper rheological properties for 3DCMP. Six different mixtures (i.e., mixtures A-F) were prepared with various gradation using five different sands (0.6-1.2 mm, 0.25-0.6 mm, 0.15-0.25 mm, less than 0.15 mm and natural river sand). The gradation of mixture A followed the Fuller Thompson theory to achieve a continuous gradation system. Mixtures B and C were two different uniform-gradation mixtures with sand particles of 0.6-1.2 mm and 0.15-0.25 mm respectively. Mixtures D and E followed the gap-gradation method, where ranges of 0.25-0.6 mm and 0.15-0.25 mm were removed respectively. Mixture F used river sand with particle size bigger than 1.2 mm sieved out.

Rheological tests illustrate that mixture A has the highest yield stresses and the lowest plastic viscosity. During the printing test for buildability, it can reach as high as 40 cm (40 layers) without notable deformation. On the contrary, all other mixtures appeared noticeable

deformation at around 30th layer. Finally, a large-scale printing with mixture A was conducted and the final printed part can be as high as 80 cm without obvious deformation. Furthermore, when mixture E with highest plastic viscosity was used for printing test, pumping pressure significantly increased compare with others. Mechanical properties, including density, compressive and flexural strength of all mixtures have also been measured.

In summary, Fuller Thompson method and Marson-Percy model can be used as the design guideline to tailor the materials to acquire appropriate rheological properties and mechanical performance for 3DCMP. More specifically, with this design guideline, desirable combination of plastic viscosity and yield stress can be achieved where low plastic viscosity is essential for good pumpability and high yield stresses for buildability. While the direct adoption of sand gradation and mix proportion in practice is not very practical due to availability of materials and other constraints, simple design guideline by adopting classic theory like Fuller Thompson method and Marson-Percy model still offers meaning insights in the further development of 3D printable material for building and construction industry.

In this research, only the sand particle gradation was investigated. In the future, it is essential to extend the gradation analysis to include other filler-like materials such as silica fume and fly ash in the fresh state. These materials contribute very little to the hydration process and therefore mainly play the role of filler like sand at least in the fresh state. Furthermore, a more quantitative link between particle size distribution/particle interactions and rheological properties needs to be established in the context of 3D printing.

Acknowledge

The authors would like to acknowledge National Research Foundation, Prime Minister's Office, Singapore under its Medium-Sized Centre funding scheme, Singapore Centre for 3D Printing and Sembcorp Design & Construction Pte Ltd for their funding and support in this research project

Appendix A

Considering a hollow cylinder has inner radius R_1 (m), outer radius R_2 (m) and height H (m), which is compressed by two plates with uniform velocity v (m/s), the coordinate can be built as shown in Fig. A. 1.

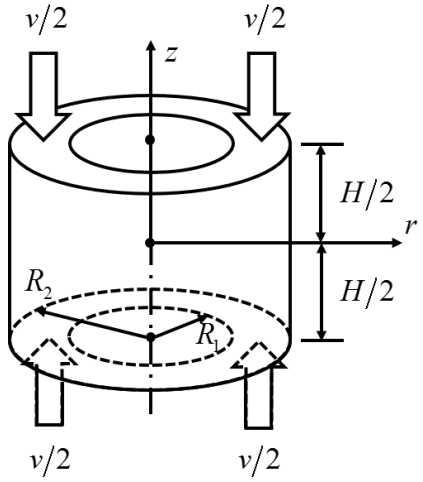

Fig. A. 1 Schematic of a hollow cylinder compressed by constant velocity.

The continuity equation under cylindrical coordinates without angular velocity can be written as

$$\frac{1}{r}\frac{\partial}{\partial r}\left(ru_r\right)+\frac{\partial u_z}{\partial z}=0 \qquad (.11)$$

where the velocities profiles on radial and axial directions satisfying governing equation and boundary conditions are

$$u_r(r,z) = \frac{v}{2H} r + \frac{C}{r} \tag{.12}$$

$$u_z(r,z) = -\frac{v}{H} z \tag{.13}$$

where C is an undetermined constant. Thus, the strain rate tensor of this flow is

$$D_{ij} = \begin{bmatrix} \frac{v}{2H} - \frac{C}{r^2} & 0 & 0 \\ 0 & \frac{v}{2H} + \frac{C}{r^2} & 0 \\ 0 & 0 & -\frac{v}{H} \end{bmatrix} \tag{.14}$$

the second invariant is

$$I_2(r,z) = \frac{3v^2}{4H^2} + \frac{C^2}{r^4} \tag{.15}$$

and the stress tensor is

$$\begin{aligned} \sigma_{ij}^{(d)} &= \frac{K_i}{\sqrt{I_2}} D_{ij} \\ &= K_i \left(\frac{3v^2}{4H^2} + \frac{C^2}{r^4} \right)^{-\frac{1}{2}} \begin{bmatrix} \frac{v}{2H} - \frac{C}{r^2} & 0 & 0 \\ 0 & \frac{v}{2H} + \frac{C}{r^2} & 0 \\ 0 & 0 & -\frac{v}{H} \end{bmatrix} \end{aligned} \tag{.16}$$

In the absence of body forces and inertial stresses, the pressure governing equation is

$$\frac{\partial p}{\partial r} = \frac{1}{r} \frac{\partial \left[r \sigma_r^{(d)} \right]}{\partial r} - \frac{\sigma_\theta^{(d)}}{r} + \frac{\partial \sigma_{rz}}{\partial z} \tag{.17}$$

Integrating Eq. (.17) on [R_1, R_2]

$$\int_{R_1}^{R_2} \frac{\partial p}{\partial r} dr = \left(\frac{v}{2H} - \frac{C}{r^2} \right) \left[\left(\frac{3v^2}{4H^2} + \frac{C^2}{r^4} \right)^{-\frac{1}{2}} K_i \right]_{R_1}^{R_2}$$

$$+ K_i \operatorname{arcsinh}\left(\sqrt{\frac{4H^2}{3v^2}} \frac{C}{r^2} \right)_{R_1}^{R_2} \qquad (.18)$$

$$= 0$$

Let $C_\alpha = HC/v$, Eq. (.18) can be rearranged as

$$\left(\frac{1}{2} - \frac{C_\alpha}{R_2^2} \right) \left(\frac{3}{4} + \frac{C_\alpha^2}{R_2^4} \right)^{-1/2} - \left(\frac{1}{2} - \frac{C_\alpha}{R_1^2} \right) \left(\frac{3}{4} + \frac{C_\alpha^2}{R_1^4} \right)^{-1/2}$$

$$+ \operatorname{arcsinh}\left(\frac{2C_\alpha}{\sqrt{3}R_2^2} \right) - \operatorname{arcsinh}\left(\frac{2C_\alpha}{\sqrt{3}R_1^2} \right) = 0 \qquad (.19)$$

Apparently, 0 is the trivial solution of Eq. (.19), another solution can be solved numerically from Eq. (.19). On the plate surface, the dissipation rate is caused by the force between plates and fluids which can be computed by

$$2 \int_{S_p} \sigma_{rz} \left(r, \frac{H}{2} \right) u_r \left(r, \frac{H}{2} \right) dS$$

$$= \frac{4\pi v K_i}{H} \left[\frac{\left(R_2^3 - R_1^3 \right)}{6} + C_\alpha \left(R_2 - R_1 \right) \right] \qquad (.20)$$

and the dissipation rate inside of the fluid can be calculated by

$$\begin{aligned}
&\int_V \sigma_{ij}^{(d)} D_{ij} dV - \int_{S_R} \sigma_{ij}^{(d)} D_{ij} dS \\
&= 2\pi v K_i C_\alpha \left(\sqrt{\frac{3R_2^4}{4C_\alpha^2} + 1} - \sqrt{\frac{3R_1^4}{4C_\alpha^2} + 1} \right) \\
&-2\pi v K_i C_\alpha \left[\operatorname{arcsinh}\left(\frac{2C_\alpha}{\sqrt{3}R_2^2} \right) - \operatorname{arcsinh}\left(\frac{2C_\alpha}{\sqrt{3}R_1^2} \right) \right] \\
&-2\pi v K_i R_1^2 \left(\frac{3}{4} + \frac{C_\alpha^2}{R_1^4} \right)^{-1/2} \left(\frac{1}{4} - \frac{C_\alpha^2}{R_1^4} \right) \\
&-2\pi v K_i R_2^2 \left(\frac{3}{4} + \frac{C_\alpha^2}{R_2^4} \right)^{-1/2} \left(\frac{1}{4} - \frac{C_\alpha^2}{R_2^4} \right)
\end{aligned} \tag{.21}$$

Therefore, the work applied on fluid is

$$\begin{aligned}
Fv = &\frac{4\pi v K_i}{H} \left[\frac{\left(R_2^3 - R_1^3 \right)}{6} + C_\alpha \left(R_2 - R_1 \right) \right] \\
&+2\pi v K_i C_\alpha \left(\sqrt{\frac{3R_2^4}{4C_\alpha^2} + 1} - \sqrt{\frac{3R_1^4}{4C_\alpha^2} + 1} \right) \\
&-2\pi v K_i C_\alpha \left[\operatorname{arcsinh}\left(\frac{2C_\alpha}{\sqrt{3}R_2^2} \right) - \operatorname{arcsinh}\left(\frac{2C_\alpha}{\sqrt{3}R_1^2} \right) \right] \\
&-2\pi v K_i R_1^2 \left(\frac{3}{4} + \frac{C_\alpha^2}{R_1^4} \right)^{-1/2} \left(\frac{1}{4} - \frac{C_\alpha^2}{R_1^4} \right) \\
&-2\pi v K_i R_2^2 \left(\frac{3}{4} + \frac{C_\alpha^2}{R_2^4} \right)^{-1/2} \left(\frac{1}{4} - \frac{C_\alpha^2}{R_2^4} \right)
\end{aligned} \tag{.22}$$

For a gravity driven hollow cylinder

$$F = \rho g H \pi \left(R_2^2 - R_1^2 \right) \tag{.23}$$

when the fluid starts to flow, it must have

$$\tau_s \alpha = \rho g H \tag{.24}$$

where

466 $$\min\left[\sigma_\theta^{(d)}\right]=\sigma_\theta^{(d)}\Big|_{r=R_2}=\tau_s \qquad (.25)$$

467 Substituting Eqs. (.23) to (.25) into Eq. (.22) and rearranging

468 $$\begin{aligned}\alpha=&\left(R_2^2-R_1^2\right)^{-1}\left(\frac{1}{2}+\frac{C_\alpha}{R_2^2}\right)^{-1}\sqrt{\frac{3}{4}+\frac{C_\alpha^2}{R_2^4}}\\&\cdot\left\{\frac{4}{H}\left[\frac{\left(R_2^3-R_1^3\right)}{6}+C_\alpha\left(R_2-R_1\right)\right]\right.\\&+2C_\alpha\left(\sqrt{\frac{3R_2^4}{4C_\alpha^2}+1}-\sqrt{\frac{3R_1^4}{4C_\alpha^2}+1}\right)\\&-2C_\alpha\left[\operatorname{arcsinh}\left(\frac{2C_\alpha}{\sqrt{3}R_2^2}\right)-\operatorname{arcsinh}\left(\frac{2C_\alpha}{\sqrt{3}R_1^2}\right)\right]\\&-2R_1^2\left(\frac{3}{4}+\frac{C_\alpha^2}{R_1^4}\right)^{-1/2}\left(\frac{1}{4}-\frac{C_\alpha^2}{R_1^4}\right)\\&\left.-2R_2^2\left(\frac{3}{4}+\frac{C_\alpha^2}{R_2^4}\right)^{-1/2}\left(\frac{1}{4}-\frac{C_\alpha^2}{R_2^4}\right)\right\}\end{aligned} \qquad (.26)$$

469 where C_α can be solved from Eq. (.19).

470 .

471 ## Reference

472 [1] C.K. Chua, K.F. Leong, C.S. Lim. Rapid Prototyping: Principles and Applications [M].
473 World Scientific Publishing Company, 2010.

474 [2] K. V. Wong, A. Hernandez, A Review of Additive Manufacturing[J]. Mechanical
475 Engineering. 2012, 1–10.

476 [3] F. Bos, R. Wolfs, Z. Ahmed, T. Salet, Additive manufacturing of concrete in construction:
477 potentials and challenges of 3D concrete printing[J]. Virtual and Physical Prototyping,
478 2016, 11(3): 209-225.

[4] S. Lim, R.A. Buswell, T.T. Le, S.A. Austin, A.G.F. Gibb, T. Thorpe, Developments in construction-scale additive manufacturing processes[J]. Automation in construction, 2012, 21: 262-268.

[5] Z, Hachem H, Tourbah A, et al. 3D concrete printing: Machine and mix design[J]. International Journal of Civil Engineering, 2015, 6(6): 14-22.

[6] J.B. Gardiner, S. Janssen, N. Kirchner. A Realisation of a Construction Scale Robotic System for 3D Printing of Complex Formwork[C]. Proceedings of the International Symposium on Automation and Robotics in Construction. Vilnius Gediminas Technical University, Department of Construction Economics & Property, 2016, 33: 1.

[7] B. Khoshnevis, D. Hwang, K.T. Yao, et al. Mega-scale fabrication by contour crafting[J]. International Journal of Industrial and Systems Engineering, 2006, 1(3): 301-320.

[8] B. Khoshnevis. Automated construction by contour crafting—related robotics and information technologies[J]. Automation in construction, 2004, 13(1): 5-19.

[9] D. Hwang, B. Khoshnevis. Concrete wall fabrication by contour crafting[C]. 21st International Symposium on Automation and Robotics in Construction (ISARC 2004), Jeju, South Korea. 2004.

[10] C. Gosselin, R. Duballet, P. Roux, et al. Large-scale 3D printing of ultra-high performance concrete–a new processing route for architects and builders[J]. Materials & Design, 2016, 100: 102-109.

[11] T.H. Pham, J.H. Lim, Q.-C. Pham, Robotic 3D-Printing for Building and Construction[C]. Proceedings of the 2nd International Conference on Progress in Additive Manufacturing

(Pro-AM 2016), 2016, 300-305.

[12] M. Hambach, D. Volkmer, Properties of 3D-printed fiber-reinforced Portland cement paste[J]. Cement and Concrete Composites, 2017, 79: 62-70.

[13] P. Feng, X. Meng, H. Zhang, Mechanical behavior of FRP sheets reinforced 3D elements printed with cementitious materials[J]. Composite Structures, 2015, 134: 331-342.

[14] P. Feng, X. Meng, J.-F. Chen, L. Ye, Mechanical properties of structures 3D printed with cementitious powders[J]. Construction and Building Materials, 2015, 93: 486-497.

[15] T.T. Le, S.A. Austin, S. Lim, R.A. Buswell, A. Gibb, T. Thorpe, Mix design and fresh properties for high-performance printing concrete[J]. Materials and structures, 2012, 45(8): 1221-1232.

[16] R. J. Flatt, P. Bowen. Yodel: a yield stress model for suspensions[J]. Journal of the American Ceramic Society, 2006, 89(4): 1244-1256.

[17] A. Perrot, D. Rangeard, A. Pierre. Structural built-up of cement-based materials used for 3D printing extrusion techniques[J]. Materials and Structures, 2016, 49(4): 1213-1220.

[18] W.B. Ashraf, M.A. Noor, Performance-evaluation of concrete properties for different combined aggregate gradation approaches[J]. Procedia engineering, 2011, 14: 2627-2634.

[19] J. Hu, A study of effects of aggregate on concrete rheology, Ph.D.Thesis. Iowa State University, 2005 .

[20] C.L. Hwang, L.A.T. Bui, C.T. Chen, Application of Fuller's ideal curve and error function to making high performance concrete using rice husk ash[J]. Computers & Concrete, 2012, 10(6): 631-647.

[21] W.B. Fuller, S.E. Thompson. The laws of proportioning concrete[J]. Asian Journal of Civil Engineering Transport, 1907, 59:67–143.

[22] Z. Li, Advanced concrete technology[M]. John Wiley & Sons, 2011.

[23] M. Mangulkar, S. Jamkar, Review of particle packing theories used for concrete mix proportioning[J]. CONTRIBUTORY PAPERS, 2013, 4:143–148.

[24] S.A.A.M. Fennis, J.C. Walraven. Using particle packing technology for sustainable concrete mixture design[J]. Heron, 2012, 57(2): 73-101.

[25] J. Hu, K. Wang. Effect of coarse aggregate characteristics on concrete rheology[J]. Construction and Building Materials, 2011, 25(3): 1196-1204.

[26] D.M. Kalyon, S. Aktas. Factors affecting the rheology and processability of highly filled suspensions[J]. Annual review of chemical and biomolecular engineering, 2014, 5: 229-254.

[27] H.A. Barnes, J.F. Hutton, K. Walters. An introduction to rheology[M]. Elsevier, 1989.

[28] G.H. Tattersall, The rheology of Portland cement pastes[J]. British Journal of Applied Physics, 1955, 6(5): 165.

[29] C. Hu, F. De Larrard, The rheology of fresh high-performance concrete[J]. Cement and concrete research, 1996, 26(2): 283-294.

[30] Y. Weng, B. Lu, M. Tan, S. Qian, Rheology and Printability of Engineered Cementitious Composites-A Literature Review[C], Proceedings of the 2nd International Conference on Progress in Additive Manufacturing (Pro-AM 2016), 2016, 427-432.

[31] P.F.G. Banfill, G. Starrs, G. Derruau, W. McCarter, Rheology of low carbon fibre content

reinforced cement mortar[J]. Cement and Concrete Composites, 2006, 28(9): 773-780.

[32] P.F.G. Banfill, Rheology of fresh cement and concrete[J]. Rheology reviews, 2006: 61.

[33] C. Ferraris, F. De Larrard, N. Martys, S. Mindess, J. Skalny. Fresh concrete rheology: recent developments[J]. Materials Science of Concrete VI, 2001: 215-241.

[34] R.P. Chhabra and J. F. Richardson. Non-Newtonian flow and applied rheology: engineering applications. Butterworth-Heinemann, 2011.

[35] Bird, R. Byron and Dai, GC and Yarusso, Barbara J. The rheology and flow of viscoplastic materials. Reviews in Chemical Engineering, 1(1):1–70, 1983.

[36] E. Yang, M. Sahmaran, Y. YINGZI, V.C. Li. Rheological control in production of engineered cementitious composites[J]. ACI Materials Journal, 2009, 106(4): 357-366.

[37] ASTM C1611 / C1611M - 14 Standard Test Method for Slump Flow of Self-Consolidating Concrete.

[38] ASTM, C642, Standard test Method for Density, Absorption, and Voids in Hardened Concrete, Annual book of ASTM standards, vol. 4, 2006.

[39] ASTM, C109-16A, Standard Test Method for Compressive Strength of Hydraulic Cement Mortars, American Society for Testing and Materials, Philadelphia, PA, 2016.

[40] N. Roussel, C. Lanos. Plastic Fluid Flow Parameters Identification Using a Simple Squeezing Test. Applied Rheology. 2003, 13(3): 132-139